

Spin-orbital Kondo effect in a parallel double quantum dot

Yuma Okazaki,^{1,2} Satoshi Sasaki,^{1,2,*} and Koji Muraki¹

¹*NTT Basic Research Laboratories, NTT Corporation, 3-1 Morinosato-Wakamiya, Atsugi, Kanagawa 243-0198, Japan*

²*Department of Physics, Tohoku University, Sendai, Miyagi 980-8578, Japan*

(Received 4 July 2011; published 21 October 2011)

Transport properties of the two-orbital Kondo effect involving both spin and orbital (pseudospin) degrees of freedom were examined in a parallel double quantum dot with a sufficient interdot Coulomb interaction and negligibly small interdot tunneling. The Kondo effect was observed at the interdot Coulomb blockade region with degeneracies of both spin and orbital degrees of freedom. When the orbital degeneracy is lifted by applying a finite detuning, the Kondo resonance exhibits a triple-peak structure, indicating that both spin and orbital contributions are involved.

DOI: [10.1103/PhysRevB.84.161305](https://doi.org/10.1103/PhysRevB.84.161305)

PACS number(s): 73.63.Kv

The two-orbital Kondo effect is a many-body phenomenon that has been investigated for carbon-nanotube quantum dots (QDs),^{1–4} vertical QDs,⁵ and parallel double quantum dots (DQDs),^{6–17} where a localized state in the QDs has spin and orbital (pseudospin) internal degrees of freedom. Since the orbital degree of freedom plays the role of pseudospin in addition to spin, the Kondo correlation involves both spin and pseudospin-flip events, and their strong mixing leads to spin-orbital Kondo properties that are in marked contrast to an ordinary SU(2) spin-Kondo effect, in which only spin-flip events are involved.^{18–20} The spin-orbital Kondo system is characterized by an interorbital interaction V and intraorbital interaction U . Here U (V) is associated with the spin (orbital) Kondo correlation, so the ratio V/U is the critical parameter for developing a strong mixing of the spin and orbital. Experimentally, the spin-orbital Kondo effect has been observed in carbon-nanotube QDs¹ and vertical QDs,⁵ where the spin and orbital satisfy the SU(4) symmetry because $U = V$ is satisfied. On the other hand, generally $V < U$ in parallel DQDs, which consists of two capacitively coupled QDs, and the two topmost levels in each QD form a two-orbital Kondo system. This asymmetry between U and V makes it difficult to observe spin-orbital Kondo effects in this system; indeed, to the best of our knowledge, an experimental observation of such effect has not been reported.^{6–8}

In this Rapid Communication, we investigate the transport properties of the two-orbital Kondo effect in a parallel DQD in a region where both V and U are strong enough to enhance both spin and spin-orbital Kondo temperatures so that we can compare them. At a charge boundary between $(N + 1, M)$ and $(N, M + 1)$, where N (M) denotes the electron number in the left (right) dot, the two states can be regarded as up and down pseudospin states that are energetically degenerate. We focus on the case with either or both of N and M being odd, where in addition to the orbital, the spin degree of freedom naturally comes into play. Along this charge boundary, where transport should be prohibited by an interdot Coulomb interaction, we observe a Kondo-like enhancement of the conductance through the left dot characterized by a clear zero-bias peak (ZBP) and temperature scaling. As the orbital degeneracy is lifted by applying a finite detuning, the Kondo resonance splits into triple peaks, demonstrating that both spin and orbital contributions are involved. Our detuning-dependent data thus

present a crossover from a spin-orbital Kondo state in the DQD to a spin-Kondo state in the left dot.

Figure 1(a) shows our device structure. A parallel DQD is defined in a two-dimensional electron gas with density $n = 2.2 \times 10^{11} \text{ cm}^{-2}$ and mobility $\mu = 2 \times 10^6 \text{ cm}^2/\text{V s}$ confined at a GaAs/Al_{0.3}Ga_{0.7}As interface 80 nm below the surface. QDs are formed inside the two square areas enclosed by the gates, both of which are 220 nm in lithographical size. The differential conductance $G = dI/dV$ through the left QD is measured using a standard lock-in technique with 3 μV ac excitation at 78 Hz. The right dot is tunnel coupled to a single lead electrode kept at the ground and capacitively coupled to the left dot. All measurements were performed in a ³He-⁴He dilution refrigerator (the base temperature $T_b \sim 40 \text{ mK}$). The number of electrons in the left (right) QD N (M) is controlled by gate voltage V_L (V_R) applied to the gate L (R). The absolute values of N and M are determined by using a quantum point contact (QPC) charge detector. The device parameters are defined in Fig. 1(b).

The charge configuration of the DQD is determined by the on-site (U_L, U_R) and interdot (V) Coulomb interactions, which lead to a charge stability diagram exhibiting honeycomb structures as shown in Fig. 2(a). Due to on-site Coulomb blockade, a charge state (N, M) is stable inside each hexagon. At charge boundaries between (N, M) and $(N + 1, M)$ [(N, M) and $(N, M + 1)$], the two adjacent charge states are energetically degenerate, which gives rise to a single-particle resonance peak in the transport through the left (right) QD. The lines defining the left and right QD resonances are disrupted by gaps that open as a result of interdot Coulomb interaction, where different classes of charge boundaries develop between $(N, M + 1)$ and $(N + 1, M)$, as denoted by p, q, r, and s in Fig. 2(a). Consequently, in these gap regions, tunneling through an individual QD is prohibited due to interdot Coulomb interaction, which we refer to as the “interdot Coulomb blockade.” At boundaries between $(N, M + 1)$ and $(N + 1, M)$, the two states are energetically degenerate, implying that cotunneling processes retaining the total electron number in the DQD are possible. Such cotunneling events lead to a pseudospin Kondo correlation, where the charge or orbital degree of freedom plays the role of a pseudospin. The orbital degeneracies associated with these two orbitals can be classified into two types depending on

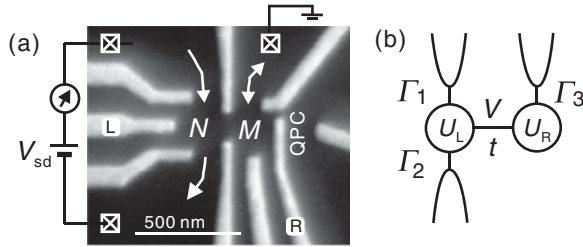


FIG. 1. (a) A scanning electron microscope image of our device. (b) Schematic diagram of our parallel dot. U_L (U_R) is on-site Coulomb interaction in the left (right) QD, and V and t are the interdot Coulomb interaction and tunneling, respectively. Γ_1 , Γ_2 , and Γ_3 are tunnel couplings to the leads. We estimate $U_L = 650 \pm 50 \mu\text{eV}$, $t \sim 20 \pm 10 \mu\text{eV}$, $\Gamma = (\Gamma_1 + \Gamma_2) \sim 260 \pm 30 \mu\text{eV}$, $\Gamma_3 \sim \Gamma = 260 \pm 30 \mu\text{eV}$, and $U_R = 1.2 \pm 0.1 \text{ meV}$ in the region of the main focus in this study.

the filling factors: 1/4 filling [p and q in Fig. 2(a)] and 1/2 filling [r and s in Fig. 2(a)].^{10,17} In the former, the spin and orbital degrees of freedom are independent, leading to fourfold degeneracy. In this case, an SU(4) Kondo effect is theoretically predicted to occur. In the latter, the four spin states associated with the (1,1) occupancy and one orbital state of (2,0) [(0,2) occupancy form fivefold degeneracy, and the pseudospin-flip events for (1,1) \leftrightarrow (2,0) [(0,2) \leftrightarrow (1,1)] can lead to a Kondo correlation [as shown in Fig. 2(b), the lower inset for the case at the (1,1)/(2,0) boundary].

Figure 2(b) shows the measured conductance through the left QD spanned by V_L and V_R . The data comprise Coulomb peaks due to transport resonance through the left QD. The Coulomb peaks are disrupted each time the electron number in the right QD changes, indicating a strong interdot Coulomb interaction in our DQD. Consequently, the charge stability diagram of the DQD is manifested by transport measurements through an individual QD. From the absolute number of electrons (N, M) in the DQD determined using the QPC charge detector, we are able to identify the filling of the topmost orbital in each QD. With the scheme shown in Fig. 2(a), each hexagonal region is thus assigned its excess electron number $(n, m) = (N - 22, M - 6)$, as shown in Fig. 2(b). Here, (22,6) is the number of inner-core electrons that do not contribute to the Kondo correlation in the relevant region. Consistent with the filling thus assigned, the on-site Coulomb blockade regions with $(n, m) = (1, m)$ show enhanced valley conductance due to the spin-Kondo effect in the left QD.

Here we focus on the region near the interdot Coulomb blockade along the (1,1)/(2,0) boundary [indicated by the dashed rectangle in Fig. 2(b)], where one expects fivefold degeneracy associated with the spin and orbital degrees of freedom for this 1/2 filling. The upper inset of Fig. 2(b) depicts the result of a detailed measurement in this region. The data demonstrate a Kondo-like conductance enhancement emerging along the (1,1)/(2,0) boundary, where transport should otherwise be prohibited by the interdot Coulomb blockade. As we detail below, we observe both ZBP and Kondo-temperature scaling for this feature, which corroborates the Kondo correlation underlying the observed conductance enhancement. The lower inset of Fig. 2(b) illustrates the possible spin configurations for each of the relevant charge

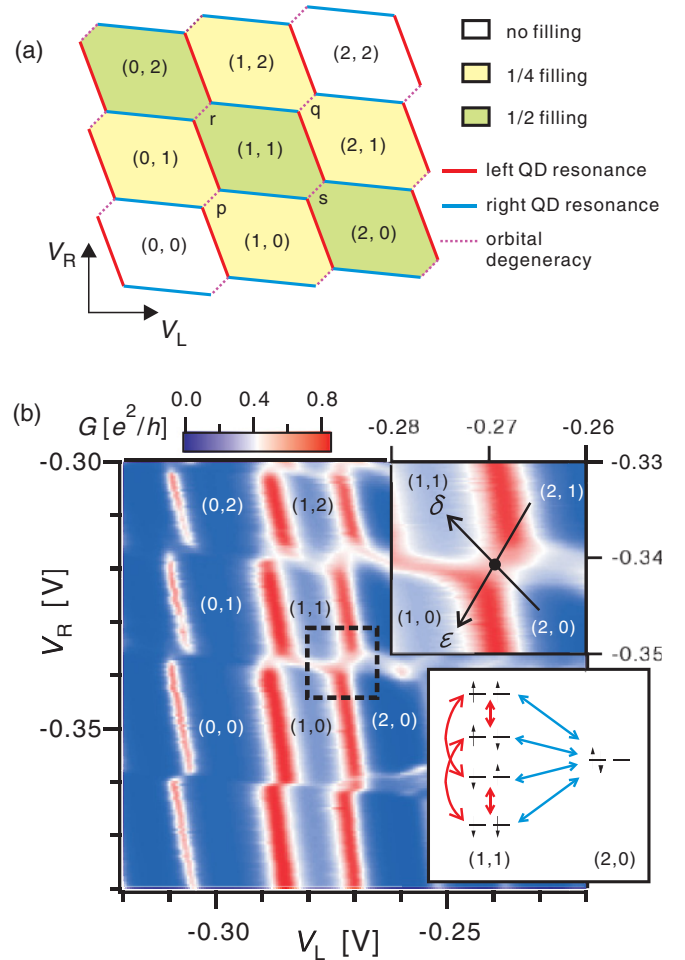


FIG. 2. (Color online) (a) Charge stability diagram and the filling factors for the topmost levels as a function of gate voltages V_L and V_R . The labels p, q, r, and s denote possible orbital degeneracy within these two orbitals. (b) Color plot of the measured differential conductance G of the left QD. The number of electrons in the topmost levels are indicated in each region. Upper inset: Detailed measurement in the area enclosed by the rectangle in the main figure. Lower inset: Spin and orbital states of fivefold degeneracy at the boundary of the (1,1)/(2,0) occupancies.

states (1,1) and (2,0). The arrows indicate possible spin- and/or pseudospin-flip processes that would contribute to the Kondo correlation.

The contributions of pseudospin and spin to the observed Kondo effect can be identified by examining the dependence of the ZBP on the detuning and magnetic field. The detuning δ , which is defined in the upper inset of Fig. 2(b), acts as an effective Zeeman energy for the pseudospin. Upon moving along the detuning axis from the (1,1)/(2,0) boundary toward the (1,1) valley center, one expects the (2,0) state to be lifted out from the fivefold degeneracy and the system to be left in fourfold degeneracy described as $\text{SU}(2) \otimes \text{SU}(2)$. Figure 3(a) depicts the evolution of the measured conductance with the source-drain bias V_{sd} and the detuning δ . The vertical dashed line in the figure marks the (1,1)/(2,0) degeneracy point (i.e., $\delta = 0$). There are two important observations to be noted. First, a ZBP (i.e., a peak at $V_{sd} = 0 \text{ V}$) exists over the entire range of δ examined. Second, as indicated by the diagonal solid lines in

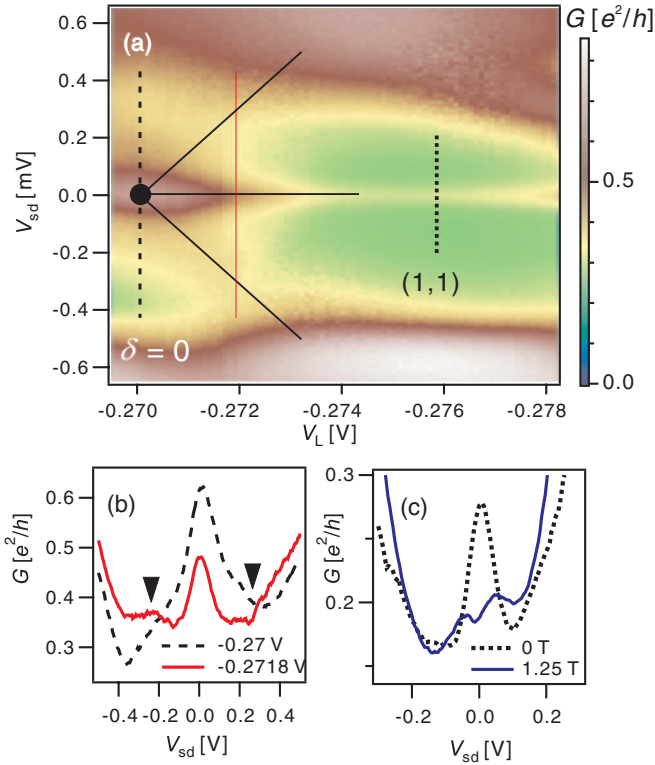


FIG. 3. (Color online) (a) Color plot of the differential conductance $G(V_{sd})$, measured along the detuning axis δ defined in the upper inset of Fig. 2(b), plotted as a function of the corresponding gate voltage V_L . (b) Detuning induced peak splitting of the Kondo resonance. The red solid (black dashed) line is extracted from (a) at $V_L = -0.2718$ V ($V_L = -0.27$ V). (c) Zeeman splitting of the Kondo resonance measured at the (1,1) valley center depicted by the black dotted line in (a). The Blue solid (black dotted) line is measured at $B = 1.25$ T ($B = 0$ T).

the figure, there are two additional features splitting off from the ZBP at the (1,1)/(2,0) degeneracy point. The persistence of the ZBP to finite δ can be understood by recalling that, even at large δ where the system is purely in the (1,1) charge configuration, the spin degeneracy in each QD is retained and so the overall fourfold degeneracy of the DQD system is preserved. The spin contribution in the Kondo state in this regime can be identified by applying an in-plane magnetic field B . As shown in Fig. 3(c), applying $B = 1.25$ T at the (1,1) valley center [vertical dotted line in Fig. 3(a)] splits the ZBP into double peaks, with their separation corresponding to the Zeeman splitting $2|g|\mu_B B$ (where $g = -0.4$ is the g factor of bulk GaAs, and μ_B is the Bohr magneton).²¹ On the other hand, the pseudospin contribution in the Kondo state at the (1,1)/(2,0) degeneracy point can be identified by applying a small detuning δ . As shown in Fig. 3(b), we observe that the ZBP splits into triple peaks when a small δ is applied. (The split-off peak for positive V_{sd} is not well resolved because of the rising background conductance.) Thus, the data in Fig. 3(a) demonstrate a crossover from a spin-orbital Kondo state involving the fivefold degeneracy of the DQD to an SU(2) spin-Kondo state in the left dot. [We note that a crossover from SU(4) to SU(2) Kondo states in a carbon-nanotube QD had been reported.³] It is interesting to note that, along with this

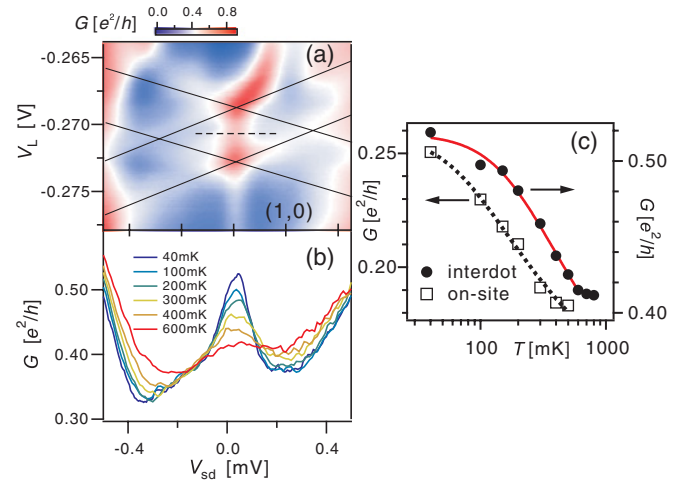


FIG. 4. (Color online) (a) Color plot of the source drain bias dependence of the differential conductance G along the ϵ axis defined in Fig. 2(b), as a function of the corresponding gate voltage V_L . (b) Zero-bias peak for different temperatures measured at the dashed line in (a). (c) Temperature dependence of the ZBP height at the interdot blockade (full circles) and at (1,0) valley center (open squares) for comparison. The red (gray) solid and black dotted lines are the fitting results.

crossover, the ZBP becomes narrower and its height smaller, suggesting the reduction in the Kondo temperature T_K .

We deduce the Kondo temperature by examining the temperature dependence of the ZBP. Figure 4(a) shows the V_{sd} dependence of G measured along the energy axis ϵ defined in the upper inset of Fig. 2(b). Here, we chose the ϵ axis (instead of the δ axis) in order to show the Coulomb diamond and the associated ZBP. As indicated by the solid lines in Fig. 4(a), a Coulomb diamond due to interdot Coulomb interaction, accompanied by a clear ZBP at its center, is visible. Figure 4(b) shows the ZBP for different temperatures, indicating that the ZBP is suppressed with increasing temperature. The closed circles in Fig. 4(c) depict the temperature dependence of the peak height. For comparison, the results for a similar measurement at the (1,0) on-site Coulomb blockade, where an ordinary SU(2) spin-Kondo effect occurs, are shown as open squares. We estimate the Kondo temperature using the following widely used empirical formula¹⁹

$$G(T) = G_0 \left[1 + (2^{1/s} - 1) \left(\frac{T}{T_K} \right)^2 \right]^{-s} + G_1,$$

with $s = 0.22$ the scaling parameter,²² G_0 the zero temperature conductance $G(T = 0)$, and G_1 the constant background. The solid and dotted lines in Fig. 4(c) represent the results of the fitting for the Kondo states in the interdot and on-site blockade regions, respectively. Here, we obtained $T_K = 0.9$ K with $G_1 = 0.27 e^2/h$ in the interdot blockade²³ and $T_K = 0.4$ K with $G_1 = 0.11 e^2/h$ in the on-site one, respectively.

There are two possible reasons for the larger T_K observed for the spin-orbital Kondo effect in the interdot blockade region: (i) When spin and orbital degrees of freedom satisfy the SU(4) symmetry, their strong mixing enhances the Kondo effect and yields a higher T_K , the so-called SU(4) Kondo effect.¹ A similar Kondo enhancement may be possible even

at the fivefold degeneracy where the SU(4) symmetry is no longer satisfied. (ii) T_K depends on the energy E of the single-particle states measured from the Fermi energy as $T_K(V, \Gamma) \sim \sqrt{\Gamma V} \exp[-\pi E(E + U)/\Gamma U]/2$.^{19,20} This scaling formula gives the minimum T_K at the center of the blockade ($E = -U/2$), and T_K increases toward the Coulomb peak. At the interdot blockade, the single-particle state is close to the Coulomb peak, and T_K is expected to be higher than that at the on-site blockade. From our measurements only, we cannot identify which mechanism is dominant.

So far we have focused on the interdot blockade region with $1/2$ filling, where we have demonstrated a unique Kondo effect arising from the fivefold degeneracy associated with both spin and pseudospin. For the interdot blockade regions with $1/4$ filling, where one expects an SU(4) Kondo effect, we did not observe a clear signature of a Kondo effect for the same set of dot tuning parameters. Combined with the fact that spin-Kondo features are clearly seen in the on-site Coulomb

blockade regions with $(n, m) = (1, m)$, this suggests that in the present setup the tunnel coupling Γ_3 with the right lead is not sufficient for the pseudospin flip to be mediated by the right lead. We speculate that adjusting Γ_3 appropriately while keeping the strong interdot Coulomb interaction may allow us to observe an SU(4) Kondo effect. Further investigation is necessary to address this issue.

In conclusion, we investigated the two-orbital Kondo effect in the capacitively coupled parallel DQD with sufficient interdot coupling V and negligible interdot tunneling t . We observed the Kondo effect at the interdot Coulomb blockade where spin and orbital degrees of freedom form fivefold degeneracy. The Kondo resonance was split into triple peaks at a finite detuning. From these results, we conclude that this Kondo effect involves both spin and orbital contributions.

We thank M. Eto, Y. Hirayama, T. Kubo, Y. V. Nazarov, R. Sakano, and Y. Tokura for valuable discussions.

*sasaki.s@lab.ntt.co.jp

¹P. Jarillo-Herrero, J. Kong, H. S. J. van der Zant, C. Dekker, L. P. Kouwenhoven, and S. D. Franceschi, *Nature (London)* **434**, 484 (2005).

²M.-S. Choi, R. López, and R. Aguado, *Phys. Rev. Lett.* **95**, 067204 (2005).

³A. Makarovski, A. Zhukov, J. Liu, and G. Finkelstein, *Phys. Rev. B* **75**, 241407(R) (2007).

⁴F. B. Anders, D. E. Logan, M. R. Galpin, and G. Finkelstein, *Phys. Rev. Lett.* **100**, 086809 (2008).

⁵S. Sasaki, S. Amaha, N. Asakawa, M. Eto, and S. Tarucha, *Phys. Rev. Lett.* **93**, 017205 (2004).

⁶U. Wilhelm, J. Schmid, J. Weis, and K. v. Klitzing, *Physica E* **14**, 385 (2002).

⁷A. W. Holleitner, A. Chudnovskiy, D. Pfannkuche, K. Eberl, and R. H. Blick, *Phys. Rev. B* **70**, 075204 (2004).

⁸A. Hübel, K. Held, J. Weis, and K. v. Klitzing, *Phys. Rev. Lett.* **101**, 186804 (2008).

⁹T. Pohjola, H. Schoeller, and G. Schön, *Europhys. Lett.* **54**, 241 (2001).

¹⁰L. Borda, G. Zaránd, W. Hofstetter, B. I. Halperin, and J. von Delft, *Phys. Rev. Lett.* **90**, 026602 (2003).

¹¹M. R. Galpin, D. E. Logan, and H. R. Krishnamurthy, *Phys. Rev. Lett.* **94**, 186406 (2005); *J. Phys. Condens. Matter* **18**, 6545 (2006).

¹²A. L. Chudonovskiy, *Europhys. Lett.* **71**, 672 (2005).

¹³J. Mravlje, A. Ramšak, and T. Rejec, *Phys. Rev. B* **73**, 241305(R) (2006).

¹⁴J. S. Lim, M.-S. Choi, M. Y. Choi, R. López, and R. Aguado, *Phys. Rev. B* **74**, 205119 (2006).

¹⁵T. Kubo, Y. Tokura, and S. Tarucha, *Phys. Rev. B* **77**, 041305 (2008).

¹⁶G. B. Martins and C. A. Büsser, *Physica B* **403**, 1514 (2008).

¹⁷H. Oguchi and N. Taniguchi, *J. Phys. Soc. Jpn.* **79**, 054706 (2010).

¹⁸D. Goldhaber-Gordon, H. Shtrikman, D. Mahalu, D. Abusch-Magder, U. Meirav, and M. A. Kastner, *Nature (London)* **391**, 156 (1998).

¹⁹D. Goldhaber-Gordon, J. Gores, M. A. Kastner, H. Shtrikman, D. Mahalu, and U. Meirav, *Phys. Rev. Lett.* **81**, 5225 (1998).

²⁰W. G. van der Wiel, S. De Franceschi, T. Fujisawa, J. M. Elzerman, S. Tarucha, and L. P. Kouwenhoven, *Science* **5487**, 2105 (2000).

²¹A. Kogan, S. Amasha, D. Goldhaber-Gordon, G. Granger, M. A. Kastner, and H. Shtrikman, *Phys. Rev. Lett.* **93**, 166602 (2004).

²²This is the value known for the SU(2) Kondo effect [T. A. Costi and A. C. Hewson, *J. Phys. Condens. Matter* **6**, 2519 (1994)]. Due to the lack of a scaling theory for (1,1)/(2,0) degeneracy, we tentatively used the same s value for the present case.

²³Fitting with $s \sim 1$ and the same G_1 yields $T_K \sim 0.7$ K. Both this value and $T_K = 0.9$ K for $s = 0.22$ are within a range consistent with the ratio of the ZBP width between the interdot blockade and the on-site one.